



Identification of the process damping coefficient in dry and wet machining of steel

Berend Denkena¹ · Benjamin Bergmann¹ · Lars Ellersiek¹

Received: 26 September 2022 / Accepted: 7 February 2023 / Published online: 16 February 2023
© The Author(s) 2023

Abstract

Flank face chamfers are an effective way to suppress vibrations and increase the productivity of milling processes. The underlying process damping mechanism is the so-called indentation effect. The effect describes the process damping as a result of an additional force due to the indentation of workpiece material under the flank face. In literature, this force is commonly modeled by the volume indented under the flank face and a process damping coefficient. To determine the process damping coefficient, various approaches with partly contradictory results exist. In this paper, a novel method to calculate the process damping coefficient based on process forces measurements in orthogonal cutting is applied for steel machining. The method considers ploughing effects of flank face chamfer and cutting edge rounding as well as plastic deformation effects. In the current investigation, the approach is applied to different cooling strategies, chamfer widths, and cutting speeds. The results show that the cutting speed has the most significant influence on the process damping coefficient. With increasing cutting speed, the process damping coefficient increases, which can be attributed to strain rate hardening effects.

Keywords Metal working fluid · Process damping · Orthogonal cutting · Ploughing force

1 Introduction

Chatter vibrations are one of the most common reasons for limited productivity in cutting. Besides constructive approaches, e.g., active damping systems, damping mechanisms resulting from the cutting process itself can be used to suppress chatter vibrations. These effects are summarized as process damping effects [1, 2]. The most important process damping effect is the indentation effect. The indentation effect describes additional ploughing forces due to the springback of the workpiece material under the flank face. The force acts against the vibration direction and leads to a damping effect [3]. A significantly improved stability behavior due to the indentation effect is demonstrated in literature for rounded [4–6], worn [7–10], and chamfered cutting tools [11–13]. An increase in the stability limit of more than 100% could be achieved in [8] for low spindle speeds using worn tools. An even higher increase in the stability limit of more

than 300% was achieved using chamfered cutting tools in milling [11].

The indentation force can be calculated by the model of Wu [14, 15]. The force is divided into a radial component and a tangential component, which depend on the indented volume under the flank face V , the friction coefficient on the flank face μ_{FF} , and a process damping coefficient K_{pd} .

$$F_{pd,r} = V \cdot K_{pd} \quad (1)$$

$$F_{pd,t} = \mu_{FF} V \cdot K_{pd} \quad (2)$$

A high number of publications focus on the determination of the process damping coefficient K_{pd} . In [16], 2D finite element simulations of an orthogonal cutting process were performed with a worn tool and a wavy surface. The results showed a decrease in the process damping coefficient with increasing tool wear. Experimental investigations with a worn tool in turning and an excitation of the tool by a piezo element were carried out in [17]. Wu used a workpiece-specific relationship based on experiments in [18] to calculate K_{pd} . In [19], stability limits for high and low spindle speeds were compared to determine the process damping coefficient. The results show process

✉ Lars Ellersiek
ellersiek@ifw.uni-hannover.de

¹ Institute of Production Engineering and Machine Tools (IFW), Leibniz Universität Hannover, An Der Universität 2, 30823 Garbsen, Germany

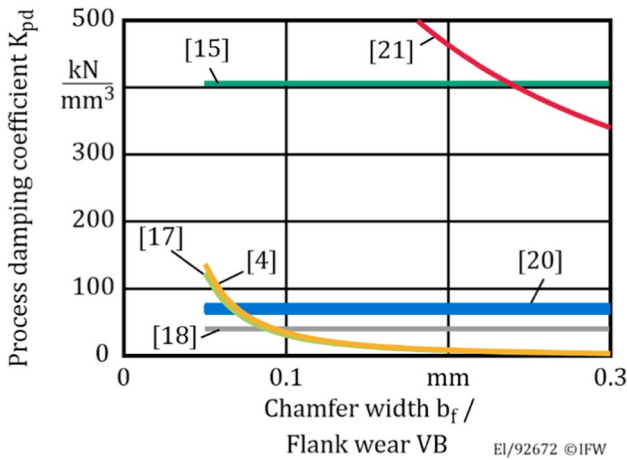


Fig. 1 Comparison of process damping coefficients identified with different approaches

damping coefficients in a range from 60 to 75 kN/mm³ for milling of steel. Sellmeier used finite element indentation tests to calculate K_{pd} [20]. An overview of different process damping coefficients K_{pd} identified in the literature for steel is given in Fig. 1.

The overview shows a strong deviation between the process damping coefficients determined in literature. Some of the investigations in literature are not based on actual cutting processes or neglect the fact that the deformation under the flank face is not pure elastic. Moreover, the influence of process-related boundary conditions, e.g., cutting speed or cooling strategy, is often not investigated. Based on the findings from literature, the research objective of this work is the knowledge of the process damping coefficient K_{pd} from actual cutting tests under the consideration of the elastic–plastic deformations under the flank face as well as process boundary conditions (cutting speed, cooling strategy).

In this paper, an approach presented in [21] to identify the process damping coefficient in the cutting of aluminium is extended. For this approach, orthogonal cutting experiments with a cutting tool with a negative chamfer angle have to be carried out. The negative chamfer angle leads to a defined indentation volume V . The general idea of the approach presented in [21] is that the process forces can be divided into the forces acting on the rake face $F_{N\gamma}$ and $F_{T\gamma}$ and the ploughing forces $F_{pd,r}$ and $F_{pd,t}$ (Fig. 2). For processes without forces acting on the flank face, the friction coefficient on the rake face can be calculated based on Eq. (3), where γ is the rake angle:

$$\frac{F_{T\gamma}}{F_{N\gamma}} = \frac{\sin(\gamma)F_c + \cos(\gamma)F_{cN}}{\cos(\gamma)F_c - \sin(\gamma)F_{cN}} = \mu_{RF} \tag{3}$$

If the ploughing forces $F_{pd,t}$ and $F_{pd,r}$ act on the flank face, they have to be subtracted from F_c and F_{cN} to calculate μ_{RF} :

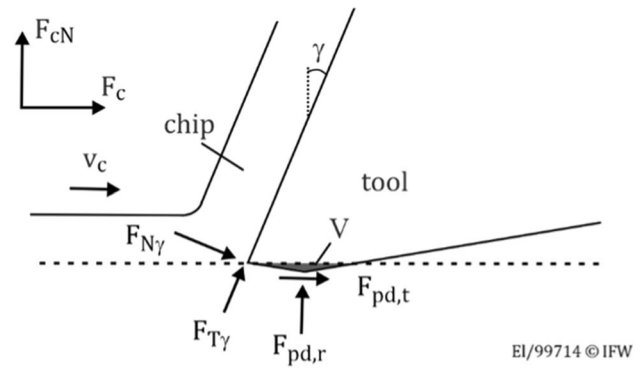


Fig. 2 Force components during orthogonal cutting [21]

$$\frac{\sin(\gamma)(F_c - F_{pd,t}) + \cos(\gamma)(F_{cN} - F_{pd,r})}{\cos(\gamma)(F_c - F_{pd,t}) - \sin(\gamma)(F_{cN} - F_{pd,r})} = \mu_{RF} \tag{4}$$

Substituting Eqs. (1) and (2) into Eq. (4) leads to Eq. (5). Note that in contrast to the work presented in [21], in this paper, a differentiation between the friction coefficient of the rake face μ_{RF} and the friction coefficient of the flank face μ_{FF} is considered:

$$\frac{\sin(\gamma)(F_c - \mu_{FF}K_{pd}V) + \cos(\gamma)(F_{cN} - K_{pd}V)}{\cos(\gamma)(F_c - \mu_{FF}K_{pd}V) - \sin(\gamma)(F_{cN} - K_{pd}V)} = \mu_{RF} \tag{5}$$

By rearranging Eq. (5), K_{pd} can be calculated as

$$K_{pd} = \frac{\mu_{RF}\cos(\gamma)F_c - \mu_{RF}\sin(\gamma)F_{cN} - \sin(\gamma)F_c - \cos(\gamma)F_{cN}}{V(\mu_{RF}\mu_{FF}\cos(\gamma) - \mu_{RF}\sin(\gamma) - \mu_{FF}\sin(\gamma) - \cos(\gamma))} \tag{6}$$

With this approach, no separation between cutting forces acting on the rake face and ploughing forces is necessary. The ploughing forces can be obtained by calculating the process damping coefficient with Eq. (6) and applying Eqs. (1) and (2). Furthermore, this approach has the advantage that adjustment errors in the chip thickness h can be neglected for the calculation of K_{pd} . However, in [21], neither the indentation effects of the cutting edge rounding nor plastic deformation effects, which influence the indented volume V , were considered. In the machining of steel, a certain cutting edge rounding is necessary to prevent an initial cutting edge failure [22]. Thus, the approach is currently not applicable to steel. This challenge will be addressed in this paper by using high-speed recordings of the cutting process. This enables the identification of the minimum chip thickness and the elastic springback and thereby a precise differentiation between elastic and plastic deformations. Moreover, there is currently no knowledge about the influence of the cooling strategy on the process damping coefficient. In this paper, the influence of various cooling strategies with different

metal working fluid (MWF) pressures and MWF mediums will be investigated for the first time using a test rig, which is specialized on high-speed recordings of cutting processes with MWF.

2 Experimental procedure and methodology

2.1 Experimental setup

To identify the process damping coefficient, orthogonal cutting experiments were performed on a planing test rig (Fig. 3a).

The test rig enables high-speed recordings (camera Photron Fastcam SA5) and force measurements (dynamometer Kistler 9257B) of processes with cutting speeds up to 500 m/min. The maximum cutting speed can be kept constant over the entire workpiece length of 120 mm. To illustrate this, the velocity and acceleration curve for the highest applied cutting speed of $v_c = 350$ m/min were calculated based on the position data of the test rig and plotted in Fig. 3b. Moreover, MWF can be applied to processes with pressures up to 70 bar by an accumulator system, which is presented in detail in [23]. The experimental setup on the planing test rig is given in Fig. 3. The MWF is applied to the process by a nozzle with a diameter $D = 1$ mm and a tilt angle $\lambda = 40^\circ$. The components of the test rig, e.g., the high-speed camera, are protected against the MWF by housing, sapphire glass, and the nozzle holder. The workpiece is mounted on the machine table, which performs a linear movement with the cutting speed. In the investigations, quenched and tempered steel AISI4140 was machined. The chip thickness h increases on the first 33 mm of the cutting process from $h = 0$ mm to a maximum uncut chip thickness $h = 0.1$ mm. The uncut chip width is $b = 2$ mm. A full factor variation of cutting speed v_c (120, 240, and 350 m/min), chamfer width b_f (130, 165, and 225 μm), MWF pressure p (10, 30, and 70 bar), and MWF medium (cutting oil Blaser Vascomill CSF35, 10% emulsion Zeller + Gmelin Zubora 67H extra) was carried out in the investigations. Furthermore, the variation of cutting speed and chamfer width was also performed for dry processes. Every experiment was repeated once. The TiAlN-coated cemented carbide tools have a negative chamfer angle $\alpha_f = -1^\circ$, a clearance angle $\alpha = 14^\circ$, a rake angle $\gamma = 1^\circ$, and a cutting edge rounding $S = 35$ μm .

2.2 Calculation of indentation volume V

In this paper, the process damping coefficient will be calculated based on process force measurements and the indented volume under the flank face according to Eq. (6). Due to the large cutting edge rounding, ploughing effects of the cutting

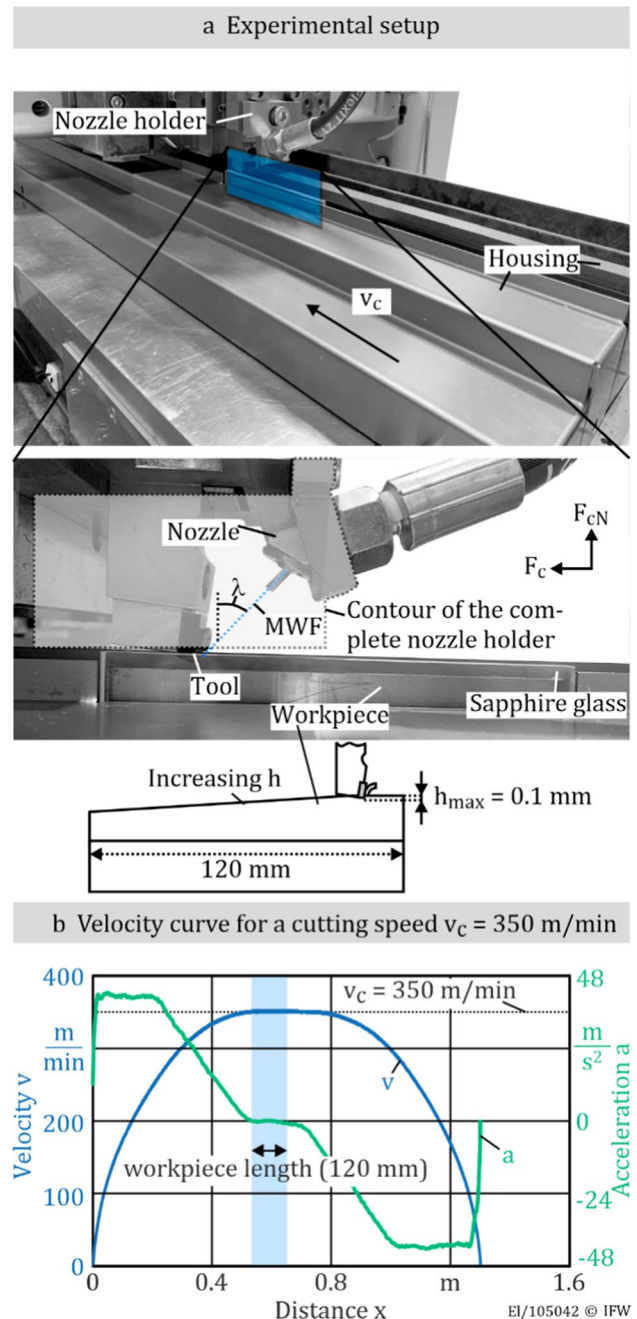


Fig. 3 a Experimental setup of the planing experiments [23] and b velocity curve for a cutting speed $v_c = 350$ m/min

edge as well as plastic deformations have to be considered. Ploughing effects on the cutting edge rounding will be considered by calculating the minimum chip thickness h_{\min} , which defines the uncut chip thickness at which the first chip formation occurs. Based on investigations in [24], the h_{\min} depends on the effective rake angle. For symmetric cutting edge microgeometries up to 100 μm , the separation point occurs at an effective rake angle of $\gamma_{h_{\min}} = -54$ to -66° . Thus, it is assumed that h_{\min} is restricted by $\gamma_{h_{\min}} = -60^\circ$,

which is shown in Fig. 4. Plastic deformation effects are considered by measuring the elastic chip thickness springback h_{el} . Overall, the indentation volume can then be calculated based on the partial areas in Fig. 4:

$$V = (A_1 + A_2 + A_3)b \tag{7}$$

The partial areas A_1 – A_3 are defined according to Eqs. (8)–(11).

$$A_1 = \frac{\bar{S}^2}{4} \left(2 \left(\frac{\pi}{2} + \gamma_{hmin} \right) - \sin \left(2 \left(\frac{\pi}{2} + \gamma_{hmin} \right) \right) \right) \tag{8}$$

$$A_2 = x_1 (b_f - \bar{S}) \left(\cos(-\alpha_f) + \frac{\sin(-\alpha_f)}{\tan(\alpha)} \right) + \frac{x_1^2}{\tan(\alpha)} + \frac{1}{2} (h_{min} - h_{el}) \left(\cos(-\alpha_f) (b_f - \bar{S}) + \frac{\sin(-\alpha_f) (b_f - \bar{S}) + x_1}{\tan(\alpha)} \right) \tag{9}$$

$$A_3 = \frac{1}{2} (b_f - \bar{S})^2 \left(\frac{\sin(-\alpha_f)}{\tan(\alpha)} + \cos(-\alpha_f) \sin(-\alpha_f) \right) \tag{10}$$

$$x_1 = \bar{S} \left(1 - \cos \left(\frac{\pi}{2} + \gamma_{hmin} \right) \right) - h_{min} + h_{el} \tag{11}$$

3 Results and discussion

3.1 Input parameters for the calculation of K_{pd}

Besides process forces measurements, the indentation volume V , the friction coefficient on the flank face μ_{FF} , and the friction coefficient on the rake face μ_{RF} are required to calculate the process damping coefficient K_{pd} according to Eq. (6).

The indentation volume V can be calculated dependent on the chamfer width b_f with the specifications of the cutting

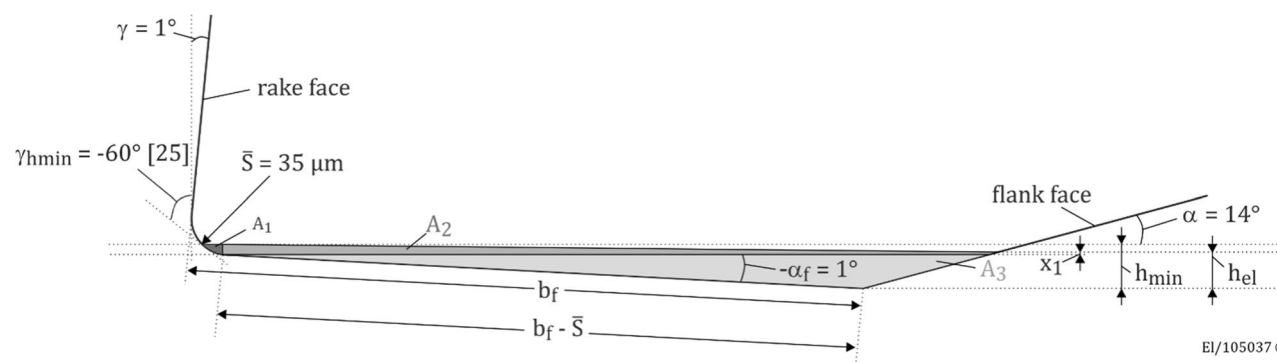


Fig. 4 Definition of the indentation area

tool ($\alpha_f = -1^\circ$, $\alpha = 14^\circ$, $\bar{S} = 35 \mu\text{m}$), the minimum chip thickness h_{min} , and the elastic chip thickness springback h_{el} .

The elastic chip thickness springback h_{el} was identified by measuring the contact length between flank face and workpiece KL_α on high-speed images during the planing process, as pictured in Fig. 5a. During a video, h_{el} was measured at five-time steps. The mean values of those measurements for the dry process are shown in Fig. 5b. With increasing chamfer width b_f , the elastic chip thickness springback increases

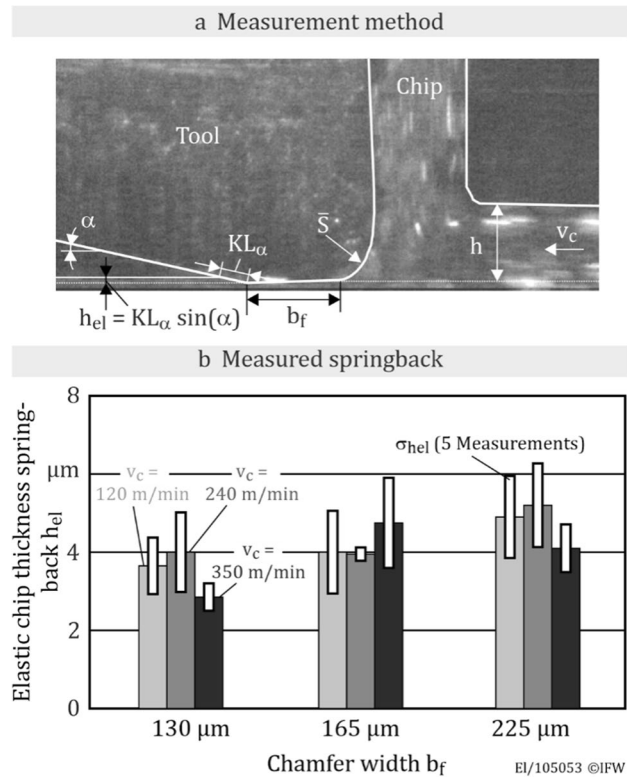


Fig. 5 a Measurement of the flank face contact length KL_α and b, measured elastic chip thickness springback h_{el} (dry)

due to an increased minimum chip thickness. On the other hand, no significant effects could be identified for the cutting speed. While the highest cutting speed leads to the lowest h_{el} at $b_f=130$ and $225 \mu\text{m}$, it also leads to the highest springback for a chamfer width $b_f=165 \mu\text{m}$. A nearly constant elastic chip thickness springback h_{el} was also shown in [25] for machining aluminum at cutting speeds $v_c \geq 150 \text{ m/min}$. This was attributed to the fact that high elastic deformations only occur at low strain rates. Due to the high ratio of tensile strength to Young’s Modulus for steel, low elastic deformations at high strain rates are also expected in this case. Since the cooling strategy also seems to have no significant influence on h_{el} , the value was only evaluated depending on the chamfer width b_f . Therefore, for the calculation of the indented volume, elastic chip thickness springbacks $h_{el} (b_f=130 \mu\text{m})=3.6 \mu\text{m}$, $h_{el} (b_f=165 \mu\text{m})=4.1 \mu\text{m}$, and $h_{el} (b_f=225 \mu\text{m})=4.7 \mu\text{m}$ are used based on the results in Fig. 5b.

The minimum chip thickness h_{min} is $4.7 \mu\text{m}$ for a symmetric cutting edge rounding $S = 35 \mu\text{m}$ and $\gamma_{hmin} = -60^\circ$. This leads to indented volumes $V (b_f=130 \mu\text{m})=0.001 \text{ mm}^3$, $V (b_f=165 \mu\text{m})=0.0014 \text{ mm}^3$, and $V (b_f=225 \mu\text{m})=0.002 \text{ mm}^3$. Nevertheless, those values are based on the averaged effective rake angle at the minimum chip thickness γ_{hmin} . In contrast, Bassett identified γ_{hmin} in a range from -54 to -66° [24]. Additional experimental results in [26] show a minimum chip thickness $h_{min}=6.7 \mu\text{m}$ at $S = 30 \mu\text{m}$ for orthogonal cutting of AISI1045, which corresponds to the boundary of Bassett’s results with $\gamma_{hmin} = -54^\circ$. Therefore, to evaluate errors in the calculation of the indented volume V , the relationship between V and γ_{hmin} is given in Fig. 6. For the boundaries of γ_{hmin} given by Bassett, a significant influence on V can be observed. The maximum relative deviations occur at the lowest chamfer width $b_f=130 \mu\text{m}$ with an increase of

31% at $\gamma_{hmin} = -54^\circ$ and a decrease of 26% at $\gamma_{hmin} = -66^\circ$. Due to the inverse proportional relationship between process damping coefficient K_{pd} and indented volume V (see Eq. (6)), those boundaries can be directly applied to the process damping coefficient K_{pd} .

The friction coefficient on the flank face μ_{FF} was calculated using force measurements during the tool entry of the chamfered tools. During the tool entry, no chip formation occurs, and the process is characterized by ploughing effects at the cutting edge and the flank face. The process forces for an unchamfered and a chamfered tool during tool entry are shown in Fig. 7. After the first contact between tool and workpiece, the forces in cutting and cutting normal direction are characterized by an almost identical increase for the unchamfered tool. When the minimum chip thickness h_{min} is exceeded, the chip formation begins. The ploughing effect is constant from this point on, and the increasing process forces are characterized by the chip formation with increasing uncut chip thickness. This leads to a higher increase of F_c compared to F_{cN} . The process forces of the chamfered tool are characterized by high cutting normal forces F_{cN}

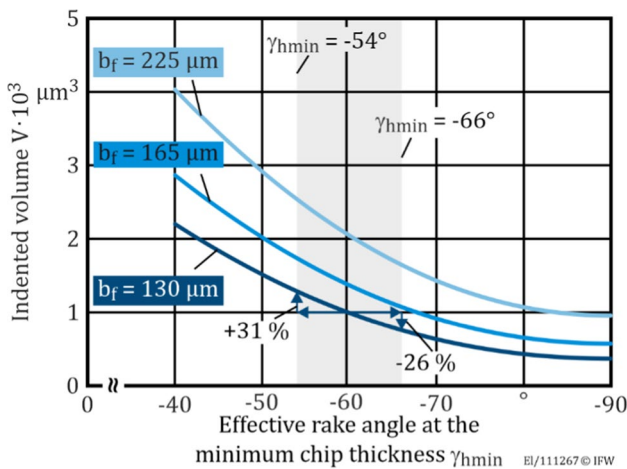


Fig. 6 Relationship between indented volume V and effective rake angle at the minimum chip thickness γ_{hmin}

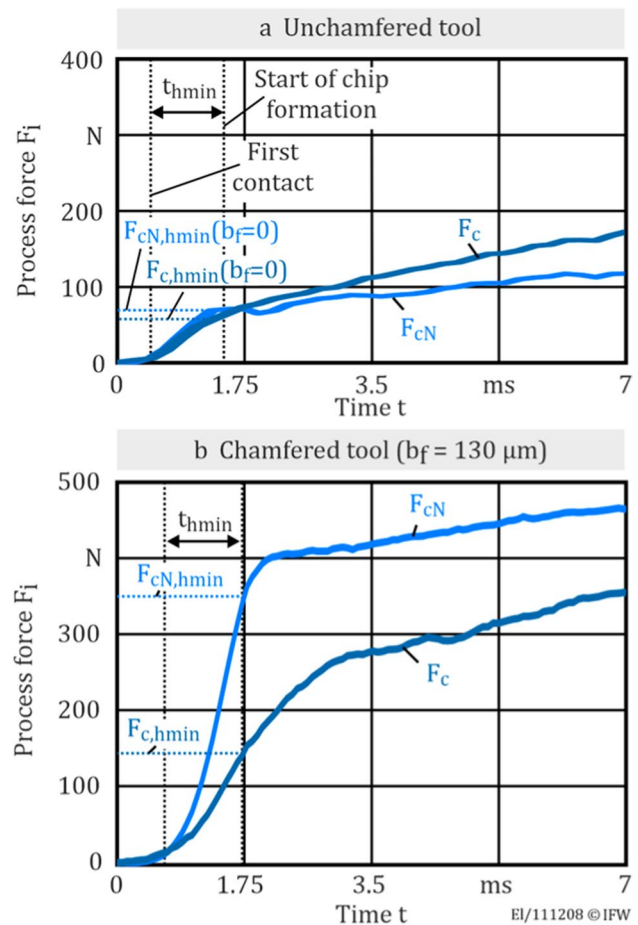


Fig. 7 a Process forces using an unchamfered tool and b process forces using a chamfered tool

after the first contact. This can be attributed to the contact between the chamfer and workpiece, which leads to additional ploughing forces in the cutting normal direction. After exceeding the minimum chip thickness h_{min} , the increase of F_c and F_{cN} is comparable to the unchamfered tool.

By subtracting the process forces of an unchamfered tool before the beginning of chip formation from the process forces of a chamfered tool, the process forces acting on the flank face can be estimated. Consequently, the friction coefficient on the flank face can be calculated using Eq. (12):

$$\mu_{FF} = \frac{(F_{cJmin} - F_{cJmin}(b_f = 0)) + (F_{cNJmin} - F_{cNJmin}(b_f = 0))\tan(-\alpha_f)}{(F_{cNJmin} - F_{cNJmin}(b_f = 0)) - (F_{cJmin} - F_{cJmin}(b_f = 0))\tan(-\alpha_f)} \quad (12)$$

For all considered processes, the friction coefficient on the flank face μ_{FF} is in a range between 0.20 and 0.29. No significant influences of chamfer width and cutting speed on μ_{FF} could be identified. Thus, the mean value over all processes $\mu_{FF} = 0.24$ was considered for the calculation of the process damping coefficient in Section 3.2.

The friction coefficient on the rake face μ_{RF} was identified based on process force measurements with an unchamfered tool. For this purpose, time-averaged values of F_c and F_{cN} for a constant uncut chip thickness $h = 0.1$ mm were used. Ploughing effects of the cutting edge rounding are taken into account by subtracting the process forces at the point of the minimum chip thickness $F_{c,hmin}$ and $F_{cN,hmin}$ from F_c and F_{cN} , respectively:

$$\mu_{RF} = \frac{(F_{cN} - F_{cN,hmin}) + (F_c - F_{c,hmin}) \cdot \tan\gamma}{(F_c - F_{c,hmin}) - (F_{cN} - F_{cN,hmin}) \cdot \tan\gamma} \quad (13)$$

The calculated friction coefficients on the rake face μ_{RF} are shown in Fig. 8a. For dry cutting processes, all cutting speeds lead to coefficients of approximately 0.5. The application of oil as MWF leads to reduced friction coefficients on the rake face at cutting speeds $v_c = 120$ m/min and pressures $p = 70$ bar. In contrast, experiments with emulsion as MWF only show a slight decrease of the friction coefficient at one process with low cutting speed $v_c = 120$ m/min and high-pressure $p = 70$ bar. In the high-speed images during the cutting process (Figs. 8b and c), it can be seen that the high MWF pressure at low cutting speed leads to visible penetration of the emulsion in the gap between chip and rake face and a turbulent flow, which might be a reason for the reduced friction coefficient. However, the formation of microfilms and the penetration of the transparent oil cannot be evaluated with high-speed images. Moreover, besides lubrication effects, changing normal loads and temperatures because of the MWF application might also influence the friction coefficient. The significant influence of metal working fluid on the cutting process can also be shown by the increasing chip thickness h' at high metal working fluid pressure. Since a higher chip thickness h' is associated with

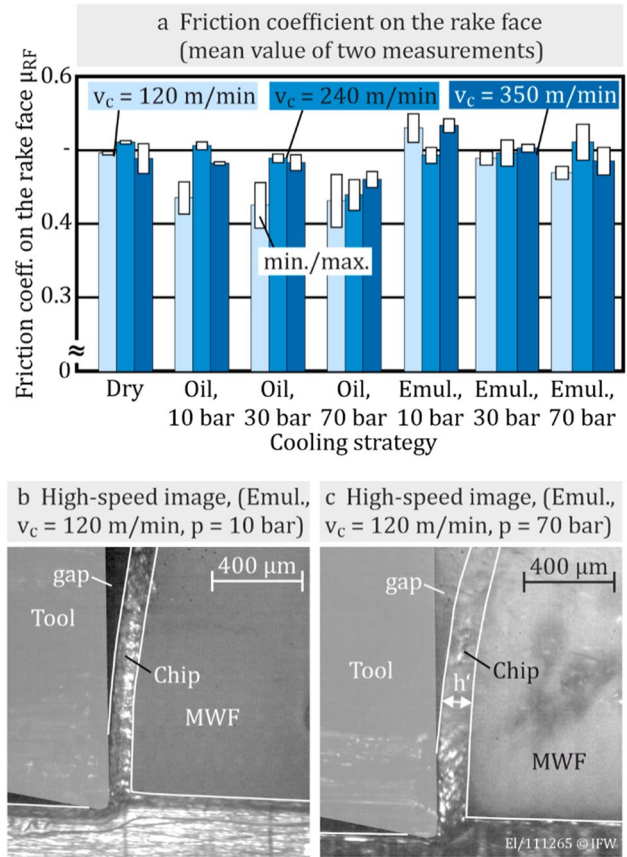


Fig. 8 a Calculated friction coefficients on the rake face, b high-speed image at low MWF pressure, and c high-speed image at high MWF pressure

a lower shear angle and, therefore, a higher friction angle and a higher friction coefficient, this is in contrast to the experimentally determined friction coefficients. A possible explanation might be the cooling effect of the high-pressure MWF, which changes the mechanical properties and, therefore, the material behavior of the workpiece.

3.2 Identified process damping coefficients

The parameters determined in Section 3.1 and process force measurements with chamfered cutting tools and constant uncut chip thickness $h = 0.1$ mm were used to calculate the process damping coefficient. The calculated process damping coefficients are shown in Fig. 9. The coefficients are in a range between 280 and 500 kN/mm^3 . Noticeable is the influence of the cutting speed. For all processes, independent of chamfer width and cooling strategy, the process damping coefficient at $v_c = 120$ m/min is smaller than the process damping coefficient at $v_c = 350$ m/min. The same effect was observed for the measured process forces. This is in contrast to thermal softening effects, which are expected with

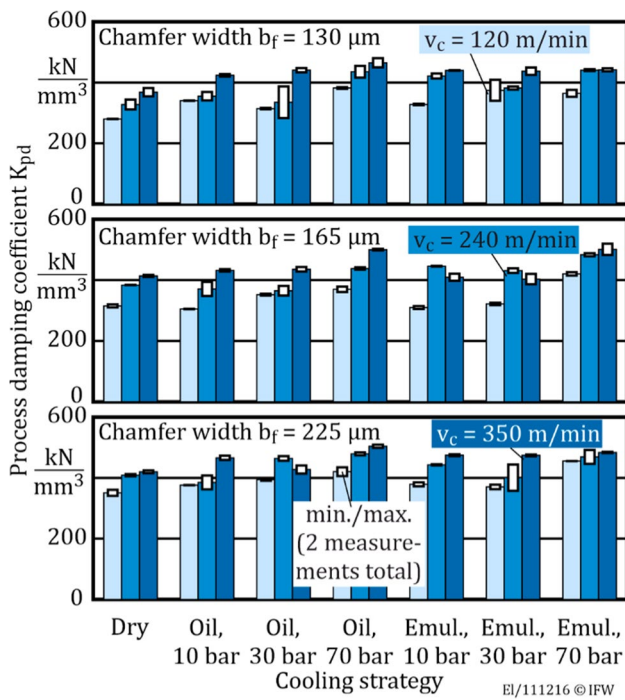


Fig. 9 Identified process damping coefficients K_{pd}

higher cutting speeds. A possible explanation is a strain rate-dependent hardening effect.

To investigate possible hardening effects, HV1 Vickers hardness measurements were conducted on the workpiece surface, which was in contact with the flank face, after the cutting process. The measurement was performed for processes with three different cutting speeds (120, 240, and 350 m/min) and two different chamfer widths (130 and 225 μm). Workpiece-specific hardness differences are considered by conducting the process and the measurement on two different workpieces. On every workpiece, three hardness measurements were carried out. The mean values of those measurements are shown in Fig. 10.

The results show that the measured hardness is higher in all cases when the surface was machined with a cutting speed of $v_c = 350 m/min$ compared to $v_c = 120 m/min$. This proves the strain rate hardening effect. Also, this effect is more dominant than thermal softening effects, which normally lead to reduced process forces with increasing cutting speed. On the other hand, no significant influences of the chamfer width on the hardness can be observed in Fig. 10.

For a further evaluation of the behavior of the process damping coefficient, a Pareto analysis was performed based on the results in Fig. 9. The results in Fig. 11 show that the cutting speed is the most significant influencing factor on the process damping coefficient. Furthermore, the effect of MWF pressure p and chamfer width b_f is also highly significant. The interactions between the individual parameters, on

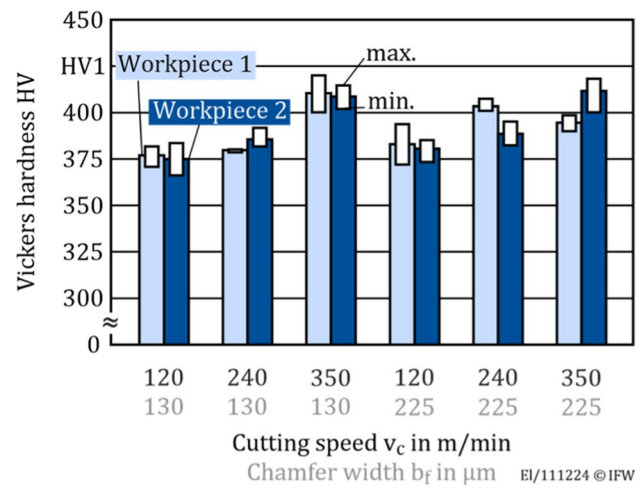


Fig. 10 Hardness measurements of workpieces machined with different cutting speeds and chamfer widths

the other hand, are not significant. The increase of the process damping coefficient K_{pd} with increasing MWF pressure p can be attributed to cooling effects. Even though the MWF is focused on the rake face, the area around the cutting edge is flooded with coolant, leading to lower material temperatures. Measurements in [27] show that Young’s modulus of the used specimen decreases from 203.5 MPa at 20 °C to 167.4 MPa at 400 °C. Thus, process forces due to material springback are reduced with higher temperatures.

An increase of the process damping coefficient K_{pd} with increasing chamfer width b_f is contrary to findings from the literature (see Fig. 1). A possible explanation is the consideration of ploughing effects and plastic deformation in this approach. An increase of the chamfer width leads to additional plastic deformation of the workpiece material, which is associated with additional forces. However, by considering the elastic chip thickness springback h_{el} in the

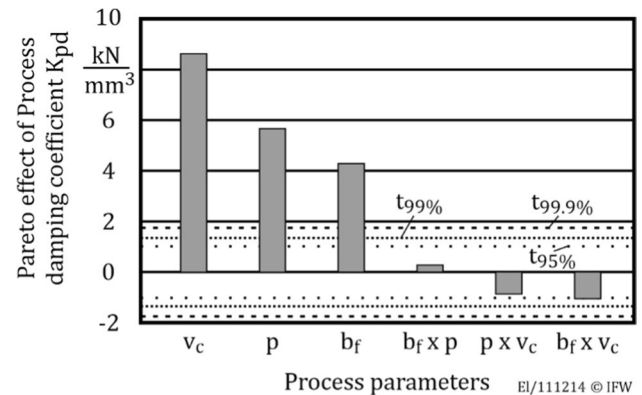


Fig. 11 Pareto effect of the process damping coefficient K_{pd}

calculation of the indented volume, only the elastic spring-back is considered in the calculation of V .

To make the results applicable for processes with different cutting speeds v_c , chamfer widths b_f , and MWF pressures p , regression models are created. The regression models are created individually for the two MWF mediums (emulsion and oil) and the dry process. As a constant factor, 212.5 kN/mm^3 was calculated over all cooling strategies. Due to the small scope of the parameter variation (only three levels per parameter), a linear dependency between the process damping coefficient K_{pd} and the parameters cutting speed v_c , chamfer width b_f and MWF pressure p was assumed. With the least squares regression method, Eq. (14) was identified for the dry cutting process, Eq. (15) was identified for cutting processes with oil as MWF, and Eq. (16) was identified for cutting processes with emulsion as MWF:

$$K_{pd} = 212,5 \frac{\text{kN}}{\text{mm}^3} + 0,525 \frac{\text{kN}}{\text{mm}^3 \cdot \mu\text{m}} b_f + 0,318 \frac{\text{kN} \cdot \text{min}}{\text{mm}^3 \cdot \text{m}} v_c \tag{14}$$

$$K_{pd} = 212,5 \frac{\text{kN}}{\text{mm}^3} + 0,447 \frac{\text{kN}}{\text{mm}^3 \cdot \mu\text{m}} b_f + 0,387 \frac{\text{kN} \cdot \text{min}}{\text{mm}^3 \cdot \text{m}} v_c + 1,0 \frac{\text{kN}}{\text{mm}^3 \cdot \text{bar}} p \tag{15}$$

$$K_{pd} = 212,5 \frac{\text{kN}}{\text{mm}^3} + 0,515 \frac{\text{kN}}{\text{mm}^3 \cdot \mu\text{m}} b_f + 0,399 \frac{\text{kN} \cdot \text{min}}{\text{mm}^3 \cdot \text{m}} v_c + 0,92 \frac{\text{kN}}{\text{mm}^3 \cdot \text{bar}} p \tag{16}$$

To evaluate the accuracy of those models, the calculated values are set against the experimental values in Fig. 12. All experimental values deviate less than 15% from the values calculated with the model. Thus, for the chosen range of cutting speed, chamfer width, and MWF pressure, the regression models have a high accuracy.

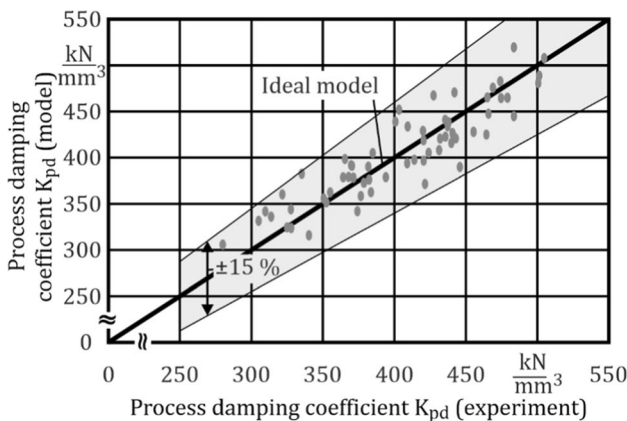


Fig. 12 Comparison of modeled and experimental identified process damping coefficient K_{pd}

The developed process damping coefficient models can be used to predict the stability behavior under the consideration of process damping effects. For the analytical prediction of the stability limit, the indented volume V can be calculated based on the velocity term \dot{x} [9]:

$$V = \frac{a_p b_f^2}{2v_c} \dot{x} \tag{17}$$

By multiplying the process damping coefficient with the indented volume V , the process damping force can be implemented in the dynamic equation.

Moreover, the stability limit can be calculated by using time-domain material removal simulations [28]. In this case, the time-resolved engagement conditions of the flank face and, subsequently, the volume indented by the flank face can be calculated. Therefore, it is possible to consider process damping effects by applying the force model of Eqs. (1) and (2).

4 Conclusions and outlook

In this paper, the process damping coefficient K_{pd} was identified using orthogonal cutting tests with a tool with a negative chamfer angle. Besides ploughing effects of the chamfer, plastic deformations and ploughing effects on the cutting edge rounding were taken into account in the analysis. The investigations were performed for different chamfer widths, cutting speeds, and cooling strategies. Based on the results, the following conclusions can be drawn:

- The friction coefficient between the flank face chamfer and workpiece (approximately 0.24) is significantly lower than the friction coefficient between chip and rake face (approximately 0.5). This can be attributed to a higher relative speed between the flank face chamfer and workpiece. Consequently, an estimated friction coefficient on the rake face is not applicable to calculate process damping forces.
- High-speed recordings enable a differentiated view on elastic–plastic deformations on the flank face. It is shown that the minimum uncut chip thickness significantly affects the indented volume V .
- The cutting speed is the most important influence factor on the process damping coefficient. With increasing cutting speed, the process damping coefficient increases. The reason is strain rate-dependent hardening effects. This effect was proven by hardness measurements of the workpiece. An increase of the cutting speed from 120 to 350 m/min leads to an increase of Vickers hardness of approximately 25 HV1.

In future investigations, the identified coefficients will be applied in a dextral-based material removal simulation [28]. Therefore, a process-specific design of the chamfer can be achieved. This might lead to a significant productivity increase. Moreover, since the investigations indicate force components due to plastic and elastic workpiece deformation, the force model might be extended by an additional term to consider the plastic deformation behavior.

Funding Open Access funding enabled and organized by Projekt DEAL. The authors would like to thank the “Sieglinde Vollmer Stiftung” for the financial support of this research work.

Data availability Raw data is available upon request.

Declarations

Conflict of interest The authors declare no competing interests.

Open Access This article is licensed under a Creative Commons Attribution 4.0 International License, which permits use, sharing, adaptation, distribution and reproduction in any medium or format, as long as you give appropriate credit to the original author(s) and the source, provide a link to the Creative Commons licence, and indicate if changes were made. The images or other third party material in this article are included in the article's Creative Commons licence, unless indicated otherwise in a credit line to the material. If material is not included in the article's Creative Commons licence and your intended use is not permitted by statutory regulation or exceeds the permitted use, you will need to obtain permission directly from the copyright holder. To view a copy of this licence, visit <http://creativecommons.org/licenses/by/4.0/>.

References

- Munoa J, Beudaert X, Dombovari Z, Altintas Y, Budak E, Brecher C, Stepan G (2016) Chatter suppression techniques in metal cutting. *CIRP Ann* 65(2):785–808
- Altintas Y (2012) *Manufacturing automation*. Cambridge University Press, Cambridge
- Sisson TR, Kegg RL (1969) An explanation of low-speed chatter effects, *Transactions of ASME. J Eng Ind* 91(4):951–958. <https://doi.org/10.1115/1.3591778>
- Ahmadi K, Altintas Y (2014) Identification of machining process damping using output-only modal analysis. *J Manuf Sci Eng* 136(5):13
- Budak E, Tunc L (2009) A new method for identification and modeling of process damping in machining. *J Manuf Sci Eng* 131(5): 051019, 10 p. <https://doi.org/10.1115/1.4000170>
- Tunc L, Budak E (2012) Effect of cutting conditions and tool geometry on process damping in machining. *Int J Mach Tools Manuf* 57:10–19
- Ahmadi K, Ismail F (2012) Stability lobes in milling including process damping and utilizing multi-frequency and semi-discretization methods, *Journal of Manufacturing. Sci Technol* 54–55:46–54
- Altintas Y, Eynian M, Onozuka H (2008) Identification of dynamic cutting force coefficients and chatter stability with process damping. *CIRP Ann Manuf Technol* 57(1):371–374
- Chiou RY, Liang SY (1998) Chatter stability of a slender cutting tool in turning with tool wear effect. *Int J Mach Tools Manuf* 38(4):315–327
- Tyler CT, Schmitz TL (2013) Analytical process damping stability prediction. *J Manuf Process* 15(1):69–76
- Sellmeier V, Denkena B (2012) High speed process damping in milling. *CIRP J Manuf Sci Technol* 5:8–19
- Denkena B, Bickel W, Grabowski R (2014) Modeling and simulation of milling processes including process damping effects. *Prod Eng Res Devel* 8(4):453–459
- Wöste F, Baumann J, Wiederkehr P, Surmann T (2019) Analysis and simulation of process damping in HPC milling. *Prod Eng Res Devel* 13(5):607–616
- Wu DW (1988) Application of a comprehensive dynamic cutting force model to orthogonal wave-generating processes. *Int J Mech Sci* 30(8):581–600
- Wu DW (1989) A new approach of formulating the transfer function for dynamic cutting processes. *J Eng Ind* 111(1):37–47. <https://doi.org/10.1115/1.3188730>
- Jin X, Altintas Y (2013) Chatter stability model of micro-milling with process damping. *J Manuf Sci Eng* 135(3):031011, 9 p. <https://doi.org/10.1115/1.4024038>
- Eynian M, Altintas Y (2009) Chatter stability of general turning operations with process damping. *J Manuf Sci Eng* 131(4):041005, 10 p. <https://doi.org/10.1115/1.3159047>
- Shaw MC, DeSalvo GJ (1970) A new approach to plasticity and its application to blunt two dimensional indenters. *ASME J Eng Ind* 92(2):469–479
- Tunc L, Budak E (2013) Identification and modeling of process damping in milling. *J Manuf Sci Eng* 131
- Sellmeier V (2012) *Über den Einfluss der Werkzeuggestalt auf die dynamische Stabilität des Fräsprozesses*, PhD Thesis, Leibniz Universität Hannover. <https://doi.org/10.15488/7976>
- Denkena B, Krödel A, Ellersiek A (2021) Determination of the process damping coefficient using plain cutting tests. *Procedia CIRP* 101:302–305
- Denkena B, Biermann D (2014) Cutting edge geometries. *CIRP Ann* 63(2):631–653
- Denkena B, Krödel A, Ellersiek L (2022) Influence of metal working fluid on chip formation and mechanical loads in orthogonal cutting. *Int J Adv Manuf Technol* 118:3005–3013
- Bassett E (2014) *Belastungsspezifische Auslegung und Herstellung von Schneidkanten für Drehwerkzeuge*, PhD Thesis, Leibniz Universität Hannover
- Schaal N, Kuster F, Wegener K (2015) Springback in metal cutting with high cutting speeds. *Procedia CIRP* 31:24–28
- Bergmann B, Denkena B, Grove T, Picker T (2019) Chip formation of rounded cutting edges. *Int J Precis Eng Manuf* 20:37–44
- Pape F, Liu H, Matthias T, Heimes N, Behrens B-A, Poll G (2021) Mechanical property determination for cutting tool and workpiece using indentation and investigations on the boundary film formed in sliding contacts with emulsions, Poster, Conference: Nanobruceken 2021, Virtual Event, Actual Science, Nanomechanical Testing Conference & Bruker Hysitron User Meeting. <https://doi.org/10.13140/RG.2.2.31717.52965>
- Denkena B, Grove T, Pape O (2019) Optimization of complex cutting tools using a multi-dextral based material removal simulation. *Procedia CIRP* 82:379–382

Publisher's note Springer Nature remains neutral with regard to jurisdictional claims in published maps and institutional affiliations.